

22 nm node wafer inspection using diffraction phase microscopy and image post-processing

Renjie Zhou^a, Gabriel Popescu^b, Lynford L. Goddard^{*a}

^aMicro and Nanotechnology Laboratory, Department of Electrical and Computer Engineering
University of Illinois at Urbana-Champaign, Urbana, Illinois 61801, USA

^bQuantitative Light Imaging Laboratory, Department of Electrical and Computer Engineering,
Beckman Institute for Advanced Science and Technology, University of Illinois at Urbana-
Champaign, Urbana, Illinois 61801, USA

Abstract

We applied epi-illumination diffraction phase microscopy to measure the amplitude and phase of the scattered field from a SEMATECH 22 nm node intentional defect array (IDA) wafer. We used several imaging processing techniques to remove the wafer's underlying structure and reduce both the spatial and temporal noise and eliminate the system calibration error to produce stretched panoramic amplitude and phase images. From the stretched images, we detected defects down to 20 nm × 160 nm for a parallel bridge, 20 nm × 100 nm for perpendicular bridge, and 35 nm × 70 nm for an isolated dot.

Keywords: Wafer defect inspection, interference microscope, phase imaging, image processing, signal to noise ratio

1. INTRODUCTION

Defect detection in semiconductor wafers is very critical for semiconductor manufacturers in order to maximize the yield. There are two main inspection methods: scanning electron microscopy (SEM) and optical microscopy. Optical microscopy is usually nondestructive which is desired for in-line inspection. However, conventional bright-field microscopy has reached its detection limit as the critical dimension (CD) of features shrinks down to 22 nm or below. In order to break the detection limit, current efforts have been focused on developing deep ultra-violet (DUV) lasers, high-order harmonic sources [1-2], and very high numerical aperture lens [3] for inspection. Actually, the ultimate limiting factor in an imaging system is the signal to noise contrast [4]. Fluorescent microscopy uses fluorescence labeled molecules to achieve intrinsic signal contrast and many super-resolution methods have been developed recently [5-7]. However, those methods are mostly point-scanning and usually there is no direct access to fluorescence in silicon wafers.

Recently, we developed wide field of view epi-illumination diffraction phase microscopy (epi-DPM) [8] and have adapted it for wafer inspection [9]. This microscopy method measures both the amplitude and phase of the scattered field using a common-path interference geometry, enabling it to be immune to vibrational noise. We have developed a sequence of image post-processing methods that reduce the spatial and temporal noise in the amplitude and phase images and improve our previous detection limit [9]. Our method has demonstrated detection of defects down to 35 nm × 70 nm for A type defects (isolated dot), 20 nm × 160 nm for BX type defects (parallel bridge) and 20 nm × 100 nm for BY type defects (perpendicular bridge) from an intentional defect array (IDA) wafer fabricated by SEMATECH. The defect detection results are confirmed by SEM.

2. EXPERIMENTAL DESIGN

Our epi-DPM microscope system is shown in Fig. 1(a). Light from a 532 nm laser first goes through a rotating diffuser to reduce speckle noise and then a linear polarizer and a half-wave plate to create linearly polarized light with an adjustable polarization axis. The linearly polarized light is normally incident on a 22 nm node IDA wafer and reflected back to the output port where the light travels through a blazed diffraction grating with 300 lines per millimeter to create multiple copies of the image. In the Fourier plane, the +1 order is low-pass filtered by a 10 μm pinhole to serve as the

*lgoddard@illinois.edu; phone 1 217 244-0799; fax 1 217 244-6375; <http://psl.mntl.illinois.edu>

reference beam, the 0 order serves as the signal, and all other orders are blocked. In the image plane, an interferogram is formed and recorded by a 16 bit charge-coupled device (CCD) camera. For wafer inspection, we translate the wafer in plane in the direction parallel to its lines in 1 micron steps and capture a sequence of images. Phase and amplitude information are then retrieved from the recorded interferograms [10].

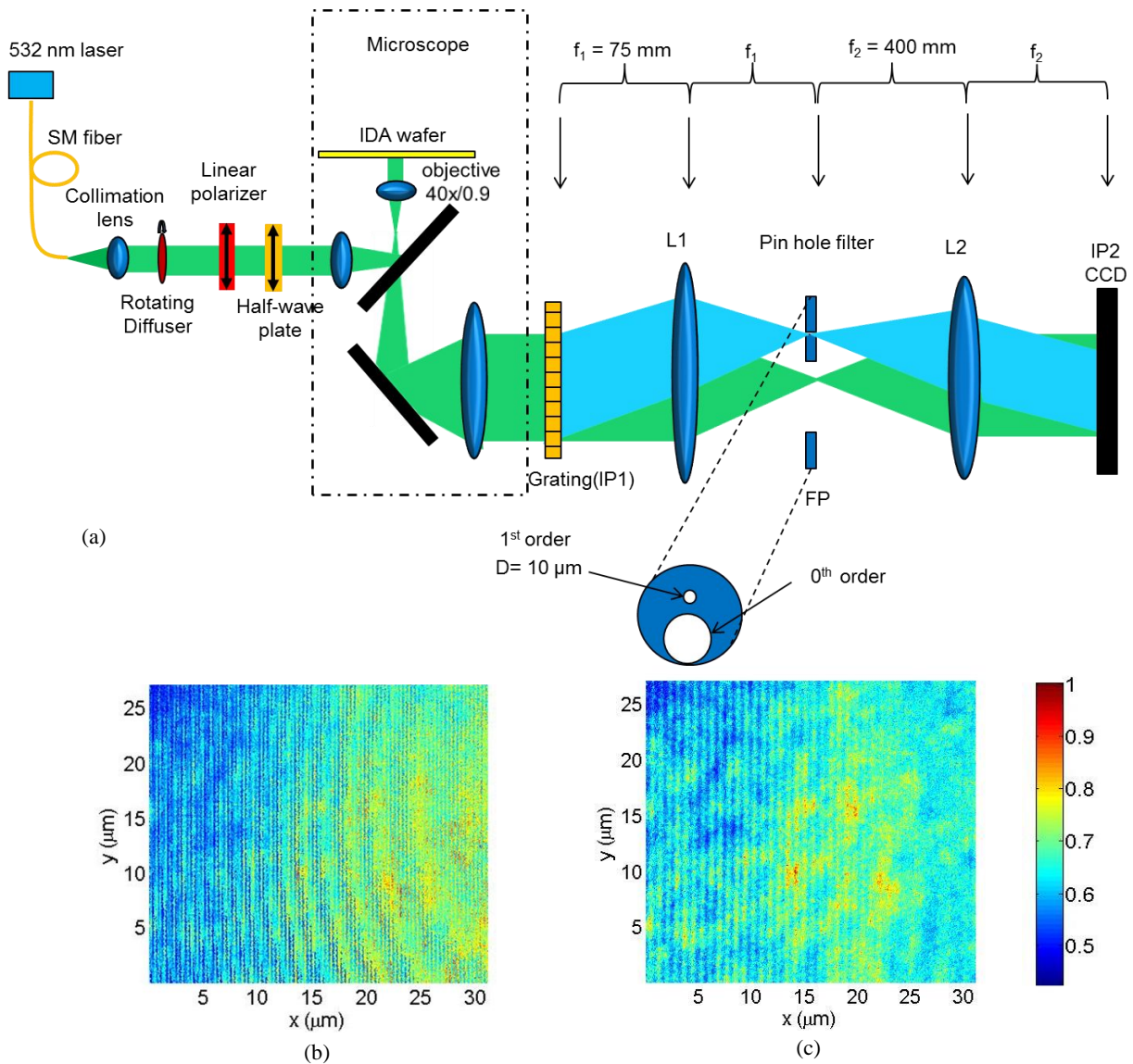


Figure 1. (a) Experimental design of the epi-DPM system. This system has a field of view of 31 μm by 27 μm and diffraction limited lateral resolution of 360 nm; (b) a typical interferogram; (c) a bright-field intensity image. Both (b) and (c) contain a defect in the center which is not visible in either image due to the noise.

In Fig. 1(b) we show a typical interferogram and in Fig. 1(c) we show a bright-field intensity image by blocking the 1st order signal. Both (b) and (c) are images of a region with a defect in the center which is not visible due to the noise resulting from laser speckle and system calibration errors. In order to reduce the noise and improve the defect signal contrast, a sequence of image post-processing method will be used. A detailed description on the processing method will be discussed in Section 4.

3. WAFER DEFECT INTRODUCTION

The IDA wafer consists of straight lines that are approximately 260 nm or 120 nm in length and 22 nm wide. The lines are arranged to form a rectangular 8-line structure which is repeated to form a 2D periodic array with 1.6 μm period [2]. Each 2D array has a total area of 100 μm by 100 μm . In the center of the 2D array, there is a printed defect. Figure 2 is an illustration of the different types of defects for a simplified IDA wafer pattern: Fig. 2(a) is an A-type defect (isolated dot), Fig. 2(b) is BY-type (perpendicular bridge) defect, and Fig. 2(c) is a BX-type (parallel bridge) defect. Each type of defect varies in size that scales against the 22 nm line-width. For example, a BX70 defect will connect the two lines in the parallel direction with a line that has 70% of the width, i.e. about 15.4 nm. There are some variations between the designed defect size and the actual printed size. So, in order to know the actual defect size, we captured SEM images of the wafer after collecting all of the epi-DPM image data. Table 1 lists the designed and measured defect sizes for some representative defects, and the relative size errors are also included in this table. Considering that the resolution of the SEM is about 5 nm, the relative size errors are within an acceptable range.

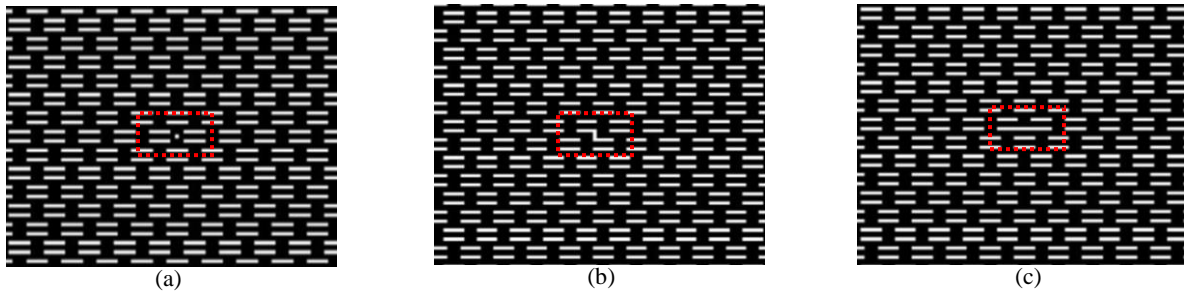


Figure 2. Illustration of different defect types. (a) is an isolated defect; (b) is a perpendicular bridge defect; and (c) is a parallel bridge defect.

Table 1. Designed and SEM measured defect sizes for representative defects.

Defect name	Designed W \times L (nm)	Measured W \times L (nm)	Error (%)
A300	66 \times 66	60 \times 90	24
BX300	66 \times 160	60 \times 160	9
BX70	15 \times 160	20 \times 160	33
BY300	66 \times 100	60 \times 100	9
BX100	22 \times 100	20 \times 100	9

4. IMAGE POST-PROCESSING METHODS

In a 2D defect array, a sequence of interferograms with 1 μm lateral sample translation between frames is collected by the CCD camera and we calculate the phase and amplitude images for each frame. In each frame, because there is strong spatial and temporal noise and system calibration error, it is not easy to detect the intentional defects. In this section, a sequence of image post-processing techniques will be used to improve the image contrast step by step to achieve reliable defect detection at the end. The techniques in sequence are: (1) calculate 2nd order differential image to remove the spatial noise, (2) perform tripole subtraction to enforce the detect signal, (3) low-pass filter to remove the noise from the underlying periodic pattern, and (4) compute a moving average to produce a stretched panoramic image using all of the scanning frames to remove temporal noise and system calibration errors. Each step will be discussed in more detail in the following, and we will only use data from BX70 array amplitude image for illustration of the intermediate image processing steps.

4.1 2nd order differential image

We start from the 1st order differential image. The 1st order differential image is defined as frame (n+1) - frame (n) where the sample has been translated parallel to the line direction by 1 μm between frames. During this subtraction, the laser speckle and the system calibration error are reduced significantly. This is because the laser speckle, which mainly originates from the surface scattering of the optical components, does not change as we move the sample. And, with a 1 micron step translation, the system response does not change and so calibration error can be removed. The resulting image is the translational difference in the structure from the wafer. The 2nd order differential image is the central difference of the first order: frame (n+1) - 2 \times frame (n) + frame (n-1). We do a 2nd order differential image because it can further reduce the spatial noise by correcting quadratic non-uniformities in the wavefront phase or amplitude. Figures 3(a)-(c) are examples of the 2nd order derivative amplitude images from the BX70 array. The defect location is marked by a red circle in each image. However, due to the underlying periodic structure and temporal noise variation, the defect signal is not yet clearly observed.

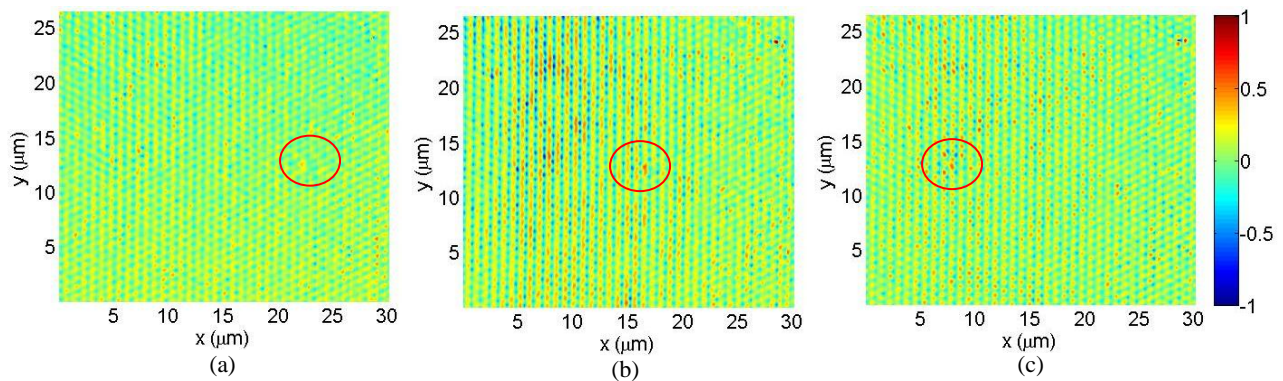


Figure 3. BX70 array 2nd order differential amplitude images with defect. (a-c) are the amplitude image of different frames. In each image, the location of the defect is marked in red circle.

4.2 Tripole subtraction

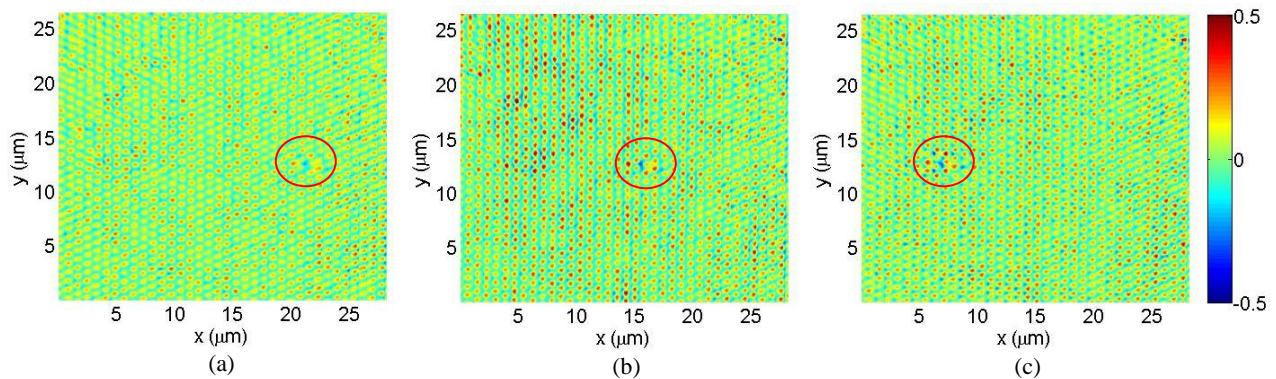


Figure 4. BX70 array tripole subtraction amplitude images using the corresponding 2nd order differential amplitude image in Fig. 3. In each image, the location of the defect is marked in red circle.

In the 2nd order differential image, the defect will be a tripole pattern. In each image, we want to extract the tripole pattern based on its period by calculating: column (j+dN) - 2 \times column (j) + column (j-dN), where column is in the translational direction, j is the column index, and dN is the wafer scan step in pixel units. As an example, if we have an original tripole cross-sectional pattern as 0 0 0 1 0 0 -2 0 0 1 0 0 0, then after tripole subtraction we obtain: 1 0 0 -4 0 0 6 0 0 -4 0 0 1. Thus, the tripole subtraction method enlarges the size and increases the defect contrast in the image.

Example tripole subtraction images are shown in Figs. 4 (a)-(c) using the corresponding 2nd order differential images in Fig. 3. From these images, the defect signal has higher contrast and becomes more visible than before.

4.3 Low-pass filtering

After the previous processing, the defect signal contrast is improved, but there is also a strong signal from the wafer's periodic structure. So, we designed a low-pass filter with cut-off right below the frequency of the wafer structure to filter the noise from the periodic pattern and maintain the signal from the defect. See Figs. 5 (a)-(c) for the filtered images from the BX70 cell using the corresponding tripole subtraction images in Fig. 4. In these filtered images, the defect tripole pattern can now be much better identified. However, considering all of the filtered scan images in the sequence, we may have false defect alarms due to the temporal noise for certain image frames. In the moving average method, we will use all of the scanning frames to do temporal noise averaging and produce a panoramic image with a high signal to noise ratio.

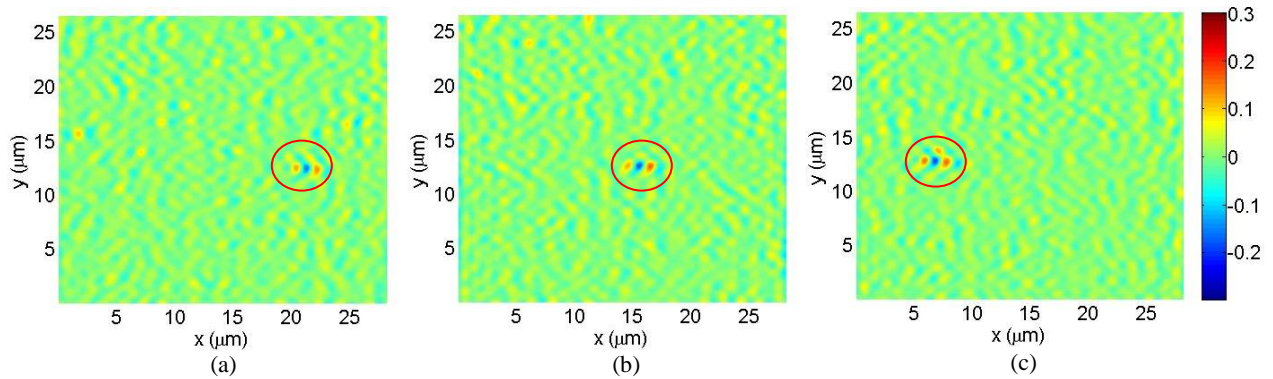


Figure 5. BX70 array tripole low-pass filtered amplitude images using the corresponding tripole subtraction amplitude image in Fig. 4. In each image, the location of the defect is marked in red circle.

4.4 Moving averaging

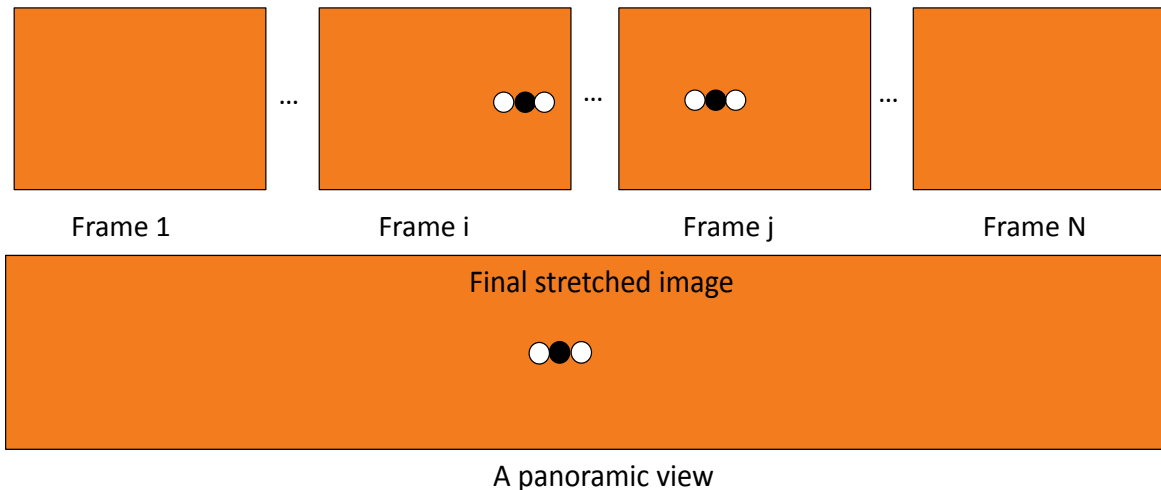


Figure 6. Illustration of moving average method. All the scanning frames are stitched together to form a stretched image with weighted averaging to reduce the temporal noise. The defect is depicted by black and white dots in a tripole pattern.

We can visually detect a defect from a sequence of scanning images by playing it as a video since the defect moves with a constant velocity, whereas the background fluctuations do not have a constant motion. To condense the video into a 2 dimensional image, we do a moving average where we first shift each frame back by the amount of the accumulated translational distance, and then add each frame together to get a stretched panoramic image, and finally average the frames by weight. See Fig. 6 for illustration. Through this averaging, the noise decreases significantly, and the signal from the defect is stabilized. In Figs. 7(a) (b), we show the amplitude and phase stretched images, respectively, using the described moving averaging method. In both images, the defect signal is very clear. Thus, the defect will be successfully detected and there will be no false alarm for defects in the whole field of view.

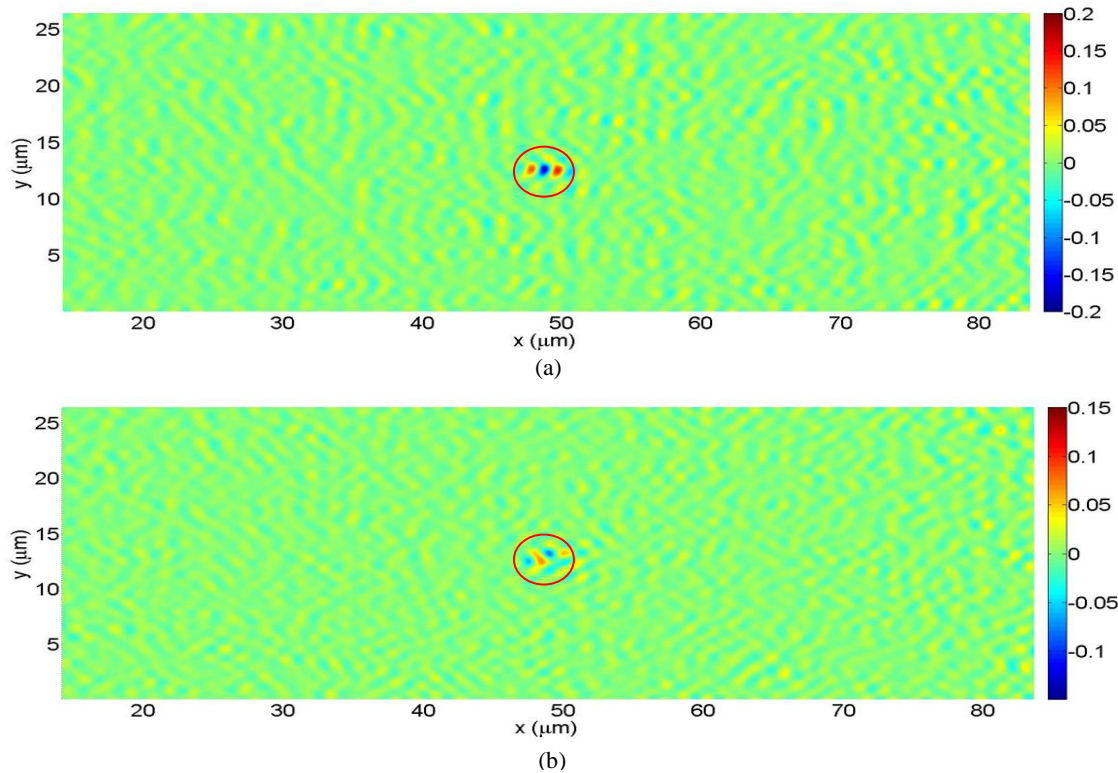


Figure 7. BX70 Stretched image using moving averaging. (a) is the stretched amplitude image and (b) is the stretched phase image. In each stretched image, the location of the defect is marked in red circle.

5. CONCLUSION

We have demonstrated defect detection using our epi-DPM system. The key to successful detection of the defects is starting with a low noise common-path quantitative phase imaging system and then performing image post-processing to further reduce the noise. Through our image post-processing, we showed that we can significantly bring down the spatial and temporal noise and the system calibration error. Defects down to BX60 (20 nm × 160 nm parallel bridge), BY100 (20 nm × 100 nm perpendicular bridge), and A200 (35 nm × 70 nm isolated dot) were successfully detected in both the final amplitude and phase stretched images. In the future, we expect to generalize our image post-processing method to detect defects in more complex and non-periodic wafers.

ACKNOWLEDGMENTS

The authors express their gratitude to SEMATECH for providing the IDA wafer. RZ would like to thank the support from Semiconductor Research Corporation (SRC) and helpful discussions with research group members from the Photonic Systems Laboratory (PSL) and Quantitative Light Imaging (QLI) Laboratory at Illinois.

REFERENCES

- [1] Seaberg, M. D., Adams, D. E., Zhang, B, Gardner, D. F., Murnane, M. M. and Kapteyn, H.C., "Ultra-high 22 nm resolution EUV coherent diffraction imaging using a tabletop 13 nm high harmonic source," Proc. SPIE 8324, 8324D (2012).
- [2] Barnes, B. M., Sohn, Y., Goasmat, F., Zhou, H., Silver, R. M. and Arceo, A., "Scatterfield microscopy of 22-nm node patterned defects using visible and DUV light," Proc. SPIE 83240, 83240F (2012).
- [3] Ippolito, S. B., Goldberg, B. B. and Unlu, M S., "High spatial resolution subsurface microscopy." Appl. Phys. Lett. 78, 4071-4073 (2001).
- [4] Zheng, G., Lee, S. A., Antebi, Y., Elowitz, M. B. and Yang, C., "The ePetri dish, an on-chip cell imaging platform based on subpixel perspective sweeping microscopy (SPSM)," Proc. Natl. Acad. Sci. USA 108, 16889 (2011).
- [5] Hell, S. W. and Wichmann, J., "Breaking the diffraction resolution limit by stimulated emission: stimulated-emission-depletion fluorescence microscopy, " Opt. Lett. 19, 780-782 (1994).
- [6] M.G.L. Gustafsson, "Nonlinear structured-illumination microscopy: wide-field fluorescence imaging with theoretically unlimited resolution, " Proc. Natl. Acad. Sci. 102, 13081–13086 (2005).
- [7] Rust, M. J., Bates, M. and Zhuang, X., "Sub-diffraction-limit imaging by stochastic optical reconstruction microscopy (STORM)," Nat. Methods 3, 793 (2006).
- [8] Edwards, C, Arbabi, A., Popescu, G. and Goddard, L. L., "Optically monitoring and controlling nanoscale topography during semiconductor etching," Light Sci. Appl 1, e30 (2012).
- [9] Zhou, R., Edwards, C., Popescu, G., and Goddard, L. L., "Diffraction Phase Microscopy for Wafer Inspection," IEEE Photonics Conference (IPC), Burlingame CA, paper WBB2 (2012).
- [10] Takahiro, I., Popescu, G., Dasari, R. R. and Feld, M. S., "Hilbert phase microscopy for investigating fast dynamics in transparent systems," Opt. Lett. 30, 1165-1167 (2005).